Understanding the remote influences of ocean weather on the episodic pulses of particulate organic carbon flux

Henry A. Ruhl[a,b,*], Frederick L. Bahr[a], Stephanie A. Henson[b], W. Brett Hosking[b], Benoit Espinola[c], Mati Kahru[d], Patrick Daniel[a], Patrick Drake[e], Christopher A Edwards[e]

[a]*Monterey Bay Aquarium Research Institute, 7700 Sandholdt Rd, Moss Landing, CA 95039, U.S.A.*
[b]*National Oceanography Centre, European Way, Southampton, SO14 3ZH, U.K.*
[c]*Ocean and Earth Science, University of Southampton, Southampton, SO14 3ZH, U.K.*
[d]*Scripps Institution of Oceanography, University of California, San Diego, La Jolla, CA 92037, U.S.A.*
[e]*Department of Ocean Science, University of California, Santa Cruz, 1156 High St, Santa Cruz, CA 95067, U.S.A.*

*Corresponding author.
E-mail address: hruhl@mbari.org (H.A. Ruhl)

Keywords: Biological carbon pump, Statistical funnel, Marine snow, Particle tracking, Ocean weather, Carbon sequestration

Highlights

Sinking marine snow and other particulate matter sequester carbon in the deep sea and provide a key food supply for life there. However, such dynamics remain challenging to quantify.

This and other recent studies highlight that the sinking speeds of particles can have important implications for the horizontal distances travelled as particles sink.

Particles with slower sinking speeds may originate from hundreds of km or more away from sediment trap sampling systems and vary from daily to inter-annual scales.

Estimating the source location can aid in assessing how conditions at these distant locations may relate to the strong variation in carbon sequestration and food resource supplies observed at time series research sites.

ABSTRACT

The biological carbon pump has been estimated to export ~5-15 Gt C yr^{-1} into the deep ocean, and forms the principal deep-sea food resource. Irregular, intense pulses of particulate organic carbon (POC) have been found to make up about one-third of the overall POC fluxes at a long-term deep-sea research station influenced by coastal upwelling of the California Current, Station M (34°50'N, 123° W, 4000 m depth). However, the drivers of these pulses have been challenging to quantify. It has long been recognized that ocean currents can result in particles being advected while sinking to the point of collection by a sediment trap. Thus, a sediment trap time series can incorporate material from a dynamic catchment area, a concept sometimes referred to as a statistical funnel. This concept raises many questions including: what are the day-to-day conditions at the source locations of the sinking POC? And, how might such 'ocean weather' and related ecosystem factors influence the intense variation seen at the seafloor? Here we analyzed three-dimensional ocean currents from a Regional Ocean Modeling System (ROMS) model from 2011-2017 to trace the potential source locations of particles sinking at 1000, 100, and 50 m d^{-1} from an export depth of 100 m. We then used regionally tailored satellite data products to estimate export flux of POC from these locations. For the 100 m d^{-1} speed, the particles had origins of up to ~300 km horizontal distance from the sediment trap location, moored at Station M at 3400 m depth., and nearly 1000 km for the 50 m d^{-1} speed. Particle tracking indicated that, there was considerable inter-annual variation in source locations. Particle source locations tended to originate from the east in the summer months, with higher export and POC fluxes. Occasionally these locations were in the vicinity of highly productive ocean features nearer to the coast. We found significant correlations between export flux of organic carbon from

the estimated source locations at 100 m depth to trap-estimated POC fluxes at 3400 m depth. These results set the stage for further investigation into sinking speed distributions, conditions at the source locations, and comparisons with mechanistic biogeochemical models and between particle tracking model frameworks.

1. Introduction

The biological carbon pump (BCP) is a complex set of processes that provides critical ecosystem functions and services including the sequestration of carbon dioxide from the atmosphere into the deep ocean where it can be removed from atmospheric climate influence for tens to thousands of years (Khatiwala et al., 2012; Fine et al., 2017). Importantly, the BCP is a critical regulator of biogeochemical rates and food resources for life in the deep ocean and on the seafloor, which make up ~97% of the oceans volume (e.g. Smith et al., 2018; Grabowski et al., 2019). Sustained observations have revealed that there can be order of magnitude variability in the year to year flux of organic carbon in the form of 'marine snow' and related detritus sinking to abyssal depths (Lampitt et al., 2010; Smith et al., 2018; Conte et al. 2018). These episodic variations are not well represented in ocean biogeochemical models and may be a source of considerable uncertainty in simulations of ocean carbon sequestration. This is partly because observing them requires high-resolution sensing and sampling over multi-year scales. In many such global biogeochemical models the flux attenuation efficiency terms are either fixed, are allowed to vary according to mean temperature, and/or oxygen concentration derived mainly in spatial terms (e.g. Cram et al., 2018; Marsay et al., 2015), or are driven by a mineral ballast framework (e.g. Armstrong et al., 2001; Yool et al., 2013). Seafloor ecological models also generally have input terms that rely on a flux that is transferred vertically (e.g. Yool et al., 2017; Durden et al., 2017). Conditions at the origin of sinking particles set the initial sinking speed and remineralization rate of particles, which may then vary before arriving at particular sampling locations and depths. Using tools that can track particles from surface to seafloor, forwards or backwards in time, can help reveal insights into the connections between surface remotely sensed properties and deep-sea time-series observations. Moreover, such insights will likely improve indicators of ecosystem conditions in a variety of applications at the scales of resource management policy implementation, such as for marine protected areas.

Since 1989, Station M has been a site for long-term biogeochemical and ecological research in the deep sea, including the fluxes of POC and Sediment Community Oxygen Consumption (SCOC). Results from the site have shown how seasonal upwelling and interannual climate variation relate to changes in surface ocean productivity, export flux and ultimately to changes in deep-sea POC fluxes and dependent communities (e.g. Smith et al., 2014; Ruhl et al., 2014). For example, the El Niño Southern Oscillation (ENSO) can relate to unusual daily conditions driving POC fluxes that are lower (during El Niño) or higher (during La Niña) than average. This has been linked to variations in upwelling, the introduction of new nutrients, and net primary production and ecological shifts in surface ocean communities (e.g. Smith et al., 2014; Lilly and Ohman, 2018). Other examples of such 'pelagic-benthic coupling' have been found in many studies including in the Arctic (Soltwedel et al., 2016), the central and northeast Atlantic (Lampitt et al., 2010; Conte et al., 2019), the Gulf of Mexico (Wei et al., 2012), continental margins (Thomsen et al., 2015) and the oligotrophic Pacific (Ruhl et al., 2008). At the Porcupine Abyssal Plain (PAP) - Sustained Observatory POC flux and variations of deep ecosystems have been linked to variations in the North Atlantic Oscillation through variability in primary productivity and surface ocean ecology (e.g. Henson et al., 2012).

Pulse events (i.e. ≥ 2 standard deviations [sd]) at Sta. M have been shown to account for about one-third of overall particulate organic carbon (POC) fluxes (Smith et al., 2018). The Martin-curve (*sensu* Martin et al. 1987) model of POC remineralization and flux estimates of POC flux to abyssal depths reproduced the background flux well at Sta. M (Smith et al., 2018).

However, the relatively episodic pulse fluxes showed major discrepancies with satellite-derived estimates, where the overall Martin-curve estimated POC flux reaching ~3400 m depth was ~50% lower than the trap estimates. Such a mis-match could have important implications for estimating the depth of carbon sequestration. In making this calculation, the export flux was estimated from satellite data for a fixed circle over the site of 100 km radius using the algorithm of Kelly et al. (2018). This approach makes the implicit assumption that sinking flux would have come from this area.

The concept of the 'statistical funnel' frames the time-series of material collected in sediment traps as coming from a dynamic catchment area where horizontal advection dominates the movement of sinking particles (Siegel and Deuser, 1997). Thus, the use of a fixed spatial integration area could miss potential particulate flux inputs coming from outside of it or dampen variation by averaging over large areas. Previous studies that simulated catchment areas and source locations of sinking particles have found that they can come from areas with contrasting conditions such as specific productivity features, coastal or offshore waters, or the presence of sea ice (e.g. Siegel et al., 2008; Hartman et al., 2010; Wekerle et al., 2018). By tracking particle trajectories across a range of sinking speeds, we can investigate if/how events from a more dynamic range of source location can account for the occasional mis-matches in estimated vs. sediment trap sampled POC fluxes to the trap depth. Indeed, particle tracking can reveal the broader range of conditions that may be related to the kind of episodic pulses of POC flux described above.

Here we seek to understand the trajectories that connect day-to-day variations in surface ocean conditions, i.e. ocean weather, to deep sediment trap time series. Specifically, we examine ocean weather in terms of daily ocean currents in a three dimensional reanalysis model (Moore et al., 2013), as well as daily satellite estimations of export flux (EF, here defined as export from 100 m depth) as determined by the new algorithm of Kahru et al. (this volume). We used these tools to address the following research questions: What are the likely source locations of EF for sinking particles reaching the deep sediment trap at Sta. M? And, how well does EF at these source locations relate to deep sediment trap samples of POC flux and SCOC? We then discuss how this first examination of particle tracking at Sta. M reveals new insights into how episodic events of POC flux at 3400 m depth might be driven by specific daily scale features of ocean circulation and EF and how they accrue into long term variation, i.e. ocean weather into ocean climate. We discuss future research directions to investigate further the role of physical, biogeochemical, and ecological variations in driving intense POC flux variations by taking advantage of tools in ocean circulation and biogeochemical models, satellite observations and *in situ* data.

2. Methods

2.1. Overall approach

We used a combination of modelled currents and particle tracking, satellite ocean color, and *in situ* sampling and sensing in the setting of the California Current. Respectively, these tools helped us to trace the possible source locations and sinking pathways of POC fluxes to Sta. M (34°50’N, 123° W, 4000 m depth). We then correlated these model and satellite estimated POC fluxes to empirical POC flux and seafloor community oxygen consumption observations.

2.2. Modeling ocean currents in three dimensions

Ocean currents were obtained from an ocean state estimate of the California Current System built on the Regional Ocean Modeling System (ROMS; Shchepetkin and McWilliams, 2004). The model domain extends from Mexico to Washington State (30 N to 48 N) and offshore to 134 W at 1/10-degree horizontal resolution and 42 terrain-following s-levels (Veneziani et al., 2009). The model data are available through the Central and Northern California Ocean Observing System (CeNCOOS). The model is forced at the surface by fields derived from the Coupled Ocean-Atmosphere Mesoscale Prediction System (COAMPS; Hodur et al., 2002; Doyle et al., 2009) and at lateral boundaries by output from the HYbrid Coordinate Ocean Model (HYCOM; Chassignet et al., 2007). The state estimate is obtained using an incremental form of the ROMS 4-dimensional variational data assimilation system (Broquet et al., 2009; Moore et al., 2011a, b) and available physical oceanographic data, including satellite derived sea surface height, sea surface temperature, and sea surface salinity, as well as *in situ* temperature and salinity from gliders and the Argo program. The model is run using the k-ω turbulence closure scheme for vertical mixing and in a series of sequential (k = kinetic energy and ω = the specific rate of dissipation of k), 4-day assimilation cycles each with 1 outer loop and 10 inner loops. Instantaneous model fields on daily intervals were used for calculations here.

2.3. Tracking particles

We used three sinking speeds representing nominally slow (50 m d^{-1}), medium (100 m d^{-1}) and fast sinking flux (1000 m d^{-1}). The speed of 100 m d^{-1} is justified from previous research on sinking speeds inferred from time lagged cross correlations between climate, upwelling, net primary production at the site (e.g. Smith et al., 2008). Similar findings have been found by Billett et al. (1983) and Lampitt et al. (1985). The 50 and 1000 m d^{-1} speeds were chosen to investigate variations that might relate to particles sinking slower in relation to smaller particles, or faster, potentially in relation to the intense pulse fluxes seen at the site (e.g. Smith et al., 2018). Such fast sinking has been estimated from Chaetognanth, Pteropod and Salp fecal pellets (Bruland and Silver, 1981; Madin, 1982; Yoon et al., 2001; reviewed in Turner, 2002), all of which occur in the study region.

The OpenDrift particle tracking python module (Dagestad et al., 2018) was used to track particle trajectories from their settling location at a deep sediment trap, backwards to their potential source location. Sets of 100 particles that were randomly seeded at 3400 m depth at longitude -123.00°E, 34.83°N on a daily basis. A random radius of 1000 m around the starting point was used. The Euler method was used for equation solutions. At each step, model data are interpolated to the advected particle's trajectory. The model was run 'backwards' using a negative time step. The Source location was determined when the particles reached 100 m depth in this 'backwards' mode. Trajectories were computed for 10 days using the 1000 m d^{-1} speed, 40 days using the 100 m d^{-1} speed and 70 days using the 50 m d^{-1} speed. Trajectory positions (latitude, longitude, and depth) are output for each day of the run.

2.4. Export flux (EF) estimation

Satellite-derived estimates of export flux of carbon (EF, mg C m^{-2} day^{-1}) were produced at daily intervals and 4 km spatial resolution (Kahru et al., this volume). Although ocean color products such as chlorophyll-a (Chl-a) are typically not available on a daily basis due to frequent cloud cover, daily estimates of net primary production (NPP, mg C m^{-2} day^{-1}) are possible as gap-free, daily satellite-derived photosynthetically active radiation (PAR, Einstein m^{-2} day^{-1}) estimates are available. In the algorithm of Kahru et al. (this volume), PAR was assumed to drive the daily variations in NPP while other components of the NPP model were assumed to change more slowly. Either 5-day interpolated Chl-a data or daily optimally interpolated products (sea surface temperature; SST) were additionally used. EF was estimated from NPP using a modification of the Kelly et al. (2018) algorithm (Kahru et al., this volume). The EF algorithm is an empirical fit to a regional *in situ* dataset of EF measurements including from near surface sediment traps and isotopic study (Stukel et al., 2019). Although the depth at which export occurs depends on mixing structure, the nominal export depth is 100 m set in part by the near surface sediment trap depth. Compared to the original Kelly et al. (2018) algorithm, the algorithm used here has a higher export efficiency (EF/NPP) and a wider dynamic range as it was fitted to a more diverse dataset including stations from active mesoscale features such as filaments and eddies.

2.5. POC flux sampling

We measured POC flux using McLane sequencing sediment traps moored at two depths: 600 and 50 m above bottom (mab). The collection time for each cup was typically ten days. Prior to deployment, the trap cups were filled with 5% buffered formalin. Upon trap recovery, zooplankton ‘swimmers’ were removed, and ¾ of the sample was freeze-dried for analysis in duplicate for total carbon (Perkin-Elmer or Exeter Analytical elemental analyzer, University of California Santa Barbara Marine Science Institute Analytical Lab) and inorganic carbon (UIC coulometer). These measurements were then corrected for salt content using $AgNO_3$ titration and used to calculate particulate organic carbon flux. We created a single time series of sediment trap sampled POC flux from a composite of the 600 and 50 mab series for use in this study. We primarily use data from the 600 mab trap (3400 m depth) when available. The 3400 m depth is therefore the depth in the ROMS model from which particles are back tracked. When 600 map trap data were not available, the time series was infilled from the 50 mab trap where possible based on the linear relationship of POC flux between these traps from 1989-2017. Further details of sample processing are provided in Smith et al. (2018).

2.6. Sediment community oxygen consumption

A benthic rover (Rover II) was used to estimate Sediment Community Oxygen Consumption (SCOC) using a pair of respiration chambers that were inserted into the sediment for approximately two day periods during its deployment from a few months to up to about one year (Smith et al., 2016). Optodes were used to measure changes in oxygen over time in the chambers, which were compared to a reference optode outside the chambers. This provided replicate SCOC estimates with a frequency of about two days while it was deployed. Results are presented in oxygen consumption equivalent terms of mg C m^{-2} d^{-1}.

2.7. Analytical approach

The location and time when particles reached a 100-m depth was recorded, here generalized as the EF depth. EF values for each of these points was then recorded for that location and time. Satellite-derived EF estimates for each of these 100 points were then recorded for that location and time. Daily average values were then computed for each of the 100 tracked particles. Two spatial integrations of EF for these daily average values were calculated at the estimated source locations: 50 and 100 km radius circles, giving a total of six independent series (three sinking speeds for each of two spatial area integrations). Given that the flux seen at the trap is a result of particles sinking at a range of speeds, we also created a series different composite weightings of the slow, medium and fast speed EF source locations. For the composites, we 1) examined a form of pulse intensity weighted composites EF set by the standard deviation (σ) of POC flux at the trap, where the fast sinking location dominated at the time of the highest σ, and slow sinking at the time of the lowest σ, and 2) vice versa. For 3), an average EF that equally valued each of the speed estimates, and a set that simply used the highest of slow, medium or fast sinking EF values from the source locations, was also created. In total there are six series at single speeds and eight series using composites of the three speeds (Table 1).

EF and POC flux data were examined at both daily and monthly scales. Months with at least 15 daily values were retained for a monthly correlation analysis. We have used the non-parametric Spearman rank correlation (r_s) to quantify correlations between EF from the various source location areas and composite weightings, and POC flux, examining the sinking speed and spatial integration series independently and as the three composite weighting of the three speeds. To account for serial autocorrelation, a correction for the degrees of freedom was applied to estimate the p values as described by Pyper and Peterman (1998). A Spearman rank correlogram was also generated to identify which parts of the time series were most correlated, which used a 13-month moving window.

3. Results

3.1. Source locations

The source locations of particles sinking at 50 and 100 m d^{-1} were not surprisingly spread over a much greater area than those sinking at 1000 m d^{-1} (Figs. 1-3). The maximum spread in the 50 m d^{-1} source locations was nearly 1000 km in its longest dimension, which ran along the California coastline. The particles generally originated from offshore waters, but did occasionally originate from near the coast. The 100 m d^{-1} source locations were nearly 300 km in both the latitudinal and longitudinal dimensions. Throughout each of the years examined there were coherent variations in the basic tendency of the source location as indicated by the monthly coloring in the location charts. The 100 m d^{-1} sinking particles also showed some considerable inter annual differences where, for example, 2013 particles tending to originate from locations to the northwest, and from late 2015 into early 2016 particles originated more often from the west. Examples of the closest coastal approaches occurred in Mar. 2011, Jan. 2014, and Nov. 2017.

3.2. Daily EF, SCOC and POC flux

EF had both notable seasonal and interannual variations, where high peaks were notably reduced or absent from 2015 and 2016 depending on the speed (e.g. Fig. 4a,b,c). Examination of the time series plots for each of the sinking speeds separately reveals when (and vial location data where) there was close correspondence (or not) to sediment trap estimated POC flux and related SCOC. The slower speeds often had higher values, in part, because locations could more frequently approach the higher productivity nearer to shore. POC flux from the integrated cup samples had a variance with peaks of up to about 12 standard deviations above the mean of 11.99 mg C m^{-2} d^{-1} for the study period. The daily SCOC was generally less variable with occasional peaks that tended to be more consistently in summer than POC flux.

3.3. Monthly time series of EF, SCOC and POC flux

Correlations of the monthly averaged time series of SCOC with the various EF estimates found that the correlations ranged from 0.51 to 0.62. (Table 1, Fig. 5). Similarly, correlation between POC flux and the EF estimates were between 0.36 and 0.55, and generally lower than with SCOC. While the coefficients show that there are some significant connections, they are sufficiently similar to preclude conclusive identification of any single speed or composite of speeds as distinctly more tightly linking the surface ocean and deep-sea carbon cycling time series. The coefficients were affected, in part, by the fact that the early part of the time series showed a relatively ‘decoupled’ relationship between EF and the deep-sea variation in SCOC and POC flux, particularly around 2012 (Fig. 5d). The period of highest correlation was in 2016 and 2017.

3.3. Seasonality in source locations and seafloor dynamics

Seasonally, the average source location was most easterly in June for the slow sinking speed and July for the medium sinking speed (Fig. 6a-f). The variance in the faster speeds was relatively little by comparison. The highest EF values were notably in July, whereas the POC flux and SCOC here generally highest from June to September (Fig. 6g-i).

4. Discussion

4.1. Particle settling from the California Current to Sta. M

The results here provide insights into the variability in source locations that can arise from different sinking speeds of marine snow particles at Sta. M. Not surprisingly, the extent of the slower sinking speed locations was much greater than the fast sinking speed. Source locations tending towards the east can bring them closer to highly productive coastal waters, upwelling jets and filaments. However, this movement in source location has considerable variation from interannual to daily scales, with indications of seasonality.

The results corroborate other studies that have found that source locations for deep-sea particulate fluxes can come from more than 100 km away. For example, investigations into the sources locations of surface waters arriving at the Porcupine Abyssal Plain (PAP) site in the Northeast Atlantic using a sea-surface oriented tracking model have found that sources were highly variable by year with origins coming from nearly 1000 km distance over 90 days

(Hartman et al., 2010). Using a combination of satellite altimeter, ship board acoustic Doppler velocity data, modeling and drifting sediment traps, Siegel et al. (2008) estimated that deep-moored traps, like those at Sta. M could have inputs coming from hundreds of km away for slower sinking speeds. Wekerle et al. (2018) estimated source locations in the Fram Strait and found that sinking speeds on the order of 100 m d^{-1} can result in particles coming from specific distant sea ice features that are thought to influence flux and vary strongly from year to year.

In the California Current Ecosystem (CCE), studies using modelled surface currents have traced upwelling events to primary production and the growth and distribution of krill patches as waters translate from nearshore to offshore over time (Messié and Chavez, 2017). A detailed process study combining field observations and three-dimensional ROMS modeling in the area overlying Station M found that subduction of particles at ocean fronts can augment sinking to enhance vertical POC flux (Stukel et al., 2017). This subduction has also been linked to substantial horizontal advection that complicates interpretations of export efficiency estimation and thus estimates of EF (Kelly et al., 2018).

The results here provide examples of how specific events of ocean weather and longer term variations can accumulate over monthly and longer timescales to drive variation in deep-sea carbon fluxes. Like other eastern boundary current systems, the California Current is known to have various scales of ecological forcing factors including ENSO, upwelling, and the formation of jets, filaments and eddies of high biological productivity moving offshore. Many of the intense peaks in EF can be traced to specific net primary production features originating at the coast and advecting offshore. In cases where there is apparent weak correspondence between EF and source locations and deep-sea POC and SCOC flux, we must recognize the limitations of EF estimation form satellite where deep chlorophyll maxima and other issues add error, as well as error in sediment trap and oxygen consumption estimation. Interannual forcing in the region also includes the influence of a relatively unusual phenomenon of large scale surface ocean warming over the greater eastern North Pacific Ocean, also known as the 'Warm Blob' that occurred from autumn 2014 to early 2016 (Bond et al., 2015; Gómez-Ocampoa et al., 2018). Its effects on the surface ocean conditions in the California Current included increased stratification, decreased chlorophyll, primary production and phytoplankton abundance (Gómez-Ocampoa et al., 2018). Source location EF values were consistently lower during this time as reflected in the 100 km composite for the highest values of the two speeds (Figs. 3 and 4). The POC flux values at abyssal depths also were consistently low for much of 2014 and 2015, although some gaps in the record do exist. The effects of the 'Warm Blob' may also have extended through to changes in the community composition of abyssal fauna (Kuhnz et al., this volume).

4.2 From initial Sta. M findings to improved understanding of the BCP

A key question arises from our findings and approach: does tracing possible source locations improve the correspondence between sediment trap variation and estimates of flux derived from satellite EF and the remineralization model of Martin et al. (1987)? We used the equation $f_z = f_{z0}(z/z_0)^{-b}$, where z_0 is export depth (here 100 m depth), f_{z0} is flux at export depth (average EF from the source locations of the three sinking speeds), and f_z is flux at depth z (here 3400-m depth), and the coefficient of flux attenuation (*b*). The *b* term here is set by the equation of Marsay et al. (2014), were $b = 0.062(x) + 0.303$ and x is the median temperature for the upper 500 m of the water column (~7.7°C at Sta. M, $b = 0.78$). For this study period of 2011-2017, the model estimated POC flux averaged 7.69 mg C m^{-2} d^{-1} whereas the trap estimated POC flux value was 12.19 mg C m^{-2} d^{-1}, a difference of 37%. As was found in Smith et al. (2018), the flux corresponded well over time except during some of the highest trap estimates (Fig. 5e).

Further investigation using particle tracking and other tools will be needed to arrive at more conclusive findings on the role of particle sinking speed and other factors in controlling in the BCP. Various combinations physical, biogeochemical and ecosystem features present several potential forms of trajectory for sinking particles (e.g. Boyd et al., 2019), some of which can be understood through the kind of modeling done here. Variation in particle size, material density, shape and water temperature could all play important roles in sinking speed (e.g. Marsay et al., 2015; Giering, 2017). The modification of particles in terms of aggregation/disaggregation and consumption and repackaging by zooplankton all add complexity to particle sinking dynamics (e.g. Burd and Jackson, 2009; Wilson et al., 2013; Cavan et al., 2018). Future work could explore the importance of sinking speeds and changes with time and depth more comprehensively. This could include setting of sinking speed distributions through models such as that described in Siegel et al. (2014). Additional formulations could look to account for the influence of strong gradients at fronts, eddy kinetic energy, and temperature, which can relate to productivity, metabolic rates and remineralization (e.g. Marsay et al., 2015), as well as viscosity (Taucher et al., 2014).

Such examinations can also compare biogeochemical fluxes in outputs from ocean biogeochemical models, such as the Model of Ecosystem Dynamics, nutrient Utilisation, Sequestration and Acidification (MEDUSA, Yool et al., 2013) or the North Pacific Ecosystem Model for Understanding Regional Oceanography (NEMURO, Kishi et al., 2007; Fiechter et al., 2014). Global climate model estimates of ocean carbon sequestration are influenced by remineralization depth (Kwon et al., 2009), which itself is partially determined by particle sinking speed. Clearer accounting for the spatio-temporal aspects of the physical, biogeochemical and ecosystem development process is beginning to help both in the interpretation of field data and its comparison to model data. For example, estimates of deep particulate carbon fluxes that are derived based on steady state assumptions of remineralization rate or sinking speed likely add considerable error (e.g. Giering et al., 2017). Vertical profiles of particle flux with depth in reality have a mix of historical influences that may extend well prior to the conditions observed at the time of collection. For example, the remnants of a spring bloom may take several weeks or more to sink. The influences of zooplankton may take even longer to manifest from their initiation, particularly for larger zooplankton that may take longer to grow. Sinking speed distributions may change over time with modification of particles via remineralization and interaction with zooplankton over time and depth.

Debate about the importance of smaller and larger particles in contributing to POC fluxes and carbon sequestration persists. This is partly because the various BCP attributes that are thought to be important are very rarely measured concurrently, and never over a seasonal bloom and carbon export cycle in high resolution (e.g. Burd et al., 2010; Briggs et al., 2011; Giering et al., 2017; Bol et al., 2018; Cavan et al., 2018). This uncertainty, in turn, limits how we might constrain a distribution of sinking speeds and related factors in modeling POC fluxes.

Blooms of diatoms and other larger phytoplankton, sinking zooplankton and their exuve, have regularly been associated with pulses of sinking POC flux (e.g. Alldredge and Gotschalk, 1989; Briggs et al. 2011, Smith 2013, 2018). Some studies have suggested that in the upper mesopelagic, most sinking POC flux may be coming from slow sinking or small particles (Alonso-González et al., 2010; Durkin et al., 2015; Villa-Alfageme et al., 2016; Baker et al., 2017). Optical and other approaches are maturing that offer promise to help quantify particle size and type distributions with depth over time, in various oceanographic settings (e.g. Lombard et al, 2019). Such data will be critical to help frame and constrain new formulations to improve model realism in quantifying sinking flux.

Monroy et al. (2019) also investigated particle sinking trajectories, in their case by seeding the model domain with a uniform particle distribution and running the sinking trajectories forward in time. This revealed that slower particles formed relatively non-uniform distributions that, when moving horizontally over time, could produce variation in fluxes without changes in the source flux of particles. This could help explain some of the intense pulse events observed at Sta. M, where fluxes might be driven to peak in relation to one of these patches of higher concentrations of sinking particles passing horizontally by a trap over a period of days or more. The initiation of a forward running particle tracking framework for the California Current will help constrain the degree to which that might be important in driving the pulses of POC flux at Sta. M.

4.3. Understanding error in model trajectories

Current data used in the models are gridded. The model includes a vertical velocity component and velocity values between grid points are calculated using interpolation techniques, which leads to approximations. Using a deterministic and mechanistic approach in this context will always yield the same result and assumes the current data and interpolation strategy to be perfect. This approach which may not account well the site’s natural variability in the velocity field. There is therefore a degree to which the model did not fully described currents in the region. This mechanistic approach can be a source of error in the trajectories of the sinking particles. A Monte-Carlo method approach introducing local variability to the interpolated values could produce a collection of possible currents in the region. The trajectory for each particle can be calculated using this collection of possible currents until they intercept a reference depth (e.g. the base of the mixed layer). This Monte-Carlo approach yields a cloud of points which define a source region (Espinola, 2018). Each of the intercepts has the same probability to be the real source for the particle. However, the point density gives the probability that a particle has originated within that region.

Additionally, the model assumes a constant vertical sinking speed with respect to the surrounding water masses. This is unlikely to reflect the speed of a particle sinking through the majority of the full-ocean water column (McDonnell and Buesseler, 2010). Particle transformation processes might either increase or decrease particle density, these complex transformations occur as the particles sink (Alldredge and Gotschalk, 1989; Armstrong et al., 2001; Boyd and Newton, 1999; Burd et al., 2010; Mayor et al., 2014; Robinson et al., 2010; Shanks and Trent, 1980; Stemmann et al., 2004). Particle remineralization is a part of these transformation processes, however, remineralization might also influence the particle size-class distribution within the flux. Slow particles that are remineralizing quickly might disappear before they can even reach the sediment trap. This might suggest that some of the particles observed in sediment trap sampling might have been modified in the water column.

4.4. Particle tracking in ocean condition indicators

Marine resource and ecosystem managers require information that is relevant for the time and space scales where management is applied. This often translates to large marine protected areas, sanctuaries and industrial lease areas that can cover areas from a few km^2 to vast areas of seafloor covering more than 100,000 km^2. These areas can experience remote influence over time (Robinson et al., 2017). The model and satellite tools used here allow for the estimation of transfers of organic carbon food resource from the surface ocean to deeper depths and the seafloor over these large scales. Such tools may help resolve questions about what drives the observed heterogeneity in seafloor ecology (Morris et al., 2016; Snelgrove et al., 2018). Model particles can be seeded at the nominal expert depth across a large study domain and then assigned a nominal sinking speed(s) and remineralization rates, to trace exported flux to depth. While there are considerable unknowns associated with sinking speed, remineralization rates and related issues, basic metric(s) for change in available energy to support ecological functions and services will likely prove valuable. Food resources at depth can then be used to drive ecological models with metrics integrated over one or more spatial domains, habitat areas, time periods or other segmentations to address management needs. For example, it will be critical to have environmental data to support the interpretation of change over time and disentangle anthropogenic impact from natural change. Spatio-temporal estimates of available food resources are critical to this. The tools used here provide a potential means to trace changes at depth to specific ocean weather and/or climatic conditions.

Acknowledgements

We would like to thank the long-time Principle Investigator for research at Sta. M, Ken Smith, as well as Crissy Huffard, Alana Sherman, Paul McGill, Richard Henthorn, John Ferreira and the many others that have contributed to making this time series work possible. Research at Sta. M during this study period is funded in part by the David and Lucile Packard Foundation. The ROMS model used as part of this study has been supported in part by CeNCOOS, the National Oceanographic Partnership Program (NOPP), the Office of Naval Research (ONR), the National Science Foundation (NSF), the National Oceanographic and Atmospheric Administration (NOAA), and the Gordon and Betty Moore Foundation. Satellite data were provided by the NASA Ocean Color Processing Group and ESA MERIS team. This work also contributes to the California Current Ecosystem - Long-Term Ecological Research (CCE-LTER) program of the National Science Foundation.

References

Alldredge, A.L., Gotschalk, C.C., 1989. Direct observations of the mass flocculation of diatom blooms: characteristics, settling velocities and formation of diatom aggregates. Deep-Sea Res. Part A 36, 159-171. https://doi.org/10.1016/0198-0149(89)90131-3.

Alonso-González, et al., 2010. Role of slowly settling particles in the ocean carbon cycle. Geophys. Res. Lett., 37, L13608, doi:10.1029/2010GL043827.

Armstrong, R.A., et al., 2001. A new, mechanistic model for organic carbon fluxes in the ocean based on the quantitative association of POC with ballast minerals. Deep-Sea Res. II, 49(1-3), 219-236. https://doi.org/10.1016/S0967-0645(01)00101-1.

Baker, C.A., et a., 2017. Slow-sinking particulate organic carbon in the Atlantic Ocean: Magnitude, flux, and potential controls. Glob. Biogeochem. Cycles, 31, 1051–1065. doi:10.1002/2017GB005638.

Bol, R., et al., 2018. High-frequency variability of small-particle carbon export flux in the Northeast Atlantic. Glob. Biogeochem. Cycles, 31. https://doi.org/10.1029/2018GB005963.

Bond, N.A., et al., 2015. Causes and impacts of the 2014 warm anomaly in the NE Pacific. Geophys. Res. Lett., 42, 3414–3420. doi:10.1002/2015GL063306.

Boyd, P.W., et al., 2019. Multi-faceted particle pumps drive carbon sequestration in the ocean. Nature 568, 327–335. https://doi.org/10.1038/s41586-019-1098-2.

Boyd, P.W., Newton, P.P., 1999. Does planktonic community structure determine downward particulate organic carbon flux in different oceanic provinces? Deep-Sea Res. I, 46(1), 63-91. https://doi.org/10.1016/S0967-0637(98)00066-1.

Briggs, N., et al., 2011. High-resolution observations of aggregate flux during a sub-polar North Atlantic spring bloom. Deep-Sea Res. I 58, 1031-1039. https://doi.org/10.1016/j.dsr.2011.07.007 .

Broquet, G., et al., 2011. Corrections to ocean sur- face forcing in the California Current System using 4D-variational data assimilation. Ocean Model. 36, 116–132. https://doi.org/10.1016/j.ocemod.2010.10.005.

Bruland, K.W., Silver, M.W., 1981. Sinking rates of fecal pellets from gelatinous zooplankton (salps, pteropods, doliolids). Mar. Biol. 63:295–300. doi: 10.1007/BF00395999.

Burd, Adrian B., et al. 2010. Assessing the apparent imbalance between geochemical and biochemical indicators of meso-and bathypelagic biological activity: What the@$]! Is wrong with present calculations of carbon budgets? Deep-Sea Res. II 57, 1557–1571. https://doi.org/10.1016/j.dsr2.2010.02.022.

Cavan, E.L., et al., 2018. Alternative particle formation pathways in the Eastern Tropical North Pacific’s biological carbon pump. J. Geophys. Res.: Biogeosci. 123, 2198–2211. https://doi.org/10.1029/2018JG004392.

Chassignet, E.P., et al., 2007. The HYCOM (HYbrid Coordinate Ocean Model) data assimilative system. J. Mar. Sys. 65, 60-83.

Conte, M.H., et al., 2019. The elemental composition of the deep particle flux in the Sargasso Sea. Chem.l Geol. 511, 279-313. https://doi.org/10.1016/j.chemgeo.2018.11.001.

Cram, J.A., et al. 2018. The Role of Particle Size, Ballast, Temperature, and Oxygen in the Sinking Flux to the Deep Sea. Glob. Biogeochem. Cycles 32, 858-876. https://doi.org/10.1029/2017GB005710.

Dagestad,K.-F., et al., 2018. OpenDrift v1.0: a generic framework for trajectory modelling. Geosci. Model Dev. 11, 1405-1420. https://doi.org/10.5194/gmd-11-1405-2018.

Doyle, J.D., et al., 2009. High-resolution real-time modeling of the marine atmospheric boundary layer in support of the AOSN-II field campaign. Deep-Sea Res. II 56, 87–99. https://doi.org/10.1016/j.dsr2.2008.08.009.

Durden, J.M., et al., 2017. Differences in the carbon flows in the benthic food webs of abyssal hill and plain habitats. Limnol. Oceanog., 62, 1771-1782. https://doi.org/10.1002/lno.10532.

Durkin, C.A., Estapa, M.L., Buesseler, K.O., 2015. Observations of carbon export by small sinking particles in the upper mesopelagic. Mar. Chem. 175, 72–81, doi:10.1016/j.marchem.2015.02.011.

Espinola, B.H.G., 2018. Neutrally buoyant sediment traps collect particles from further away than previously considered. (MSc Oceanography). University of Southampton, Southampton, UK.

Fiechter, J., et al., 2014. Air-sea CO_2 fluxes in the California Current: Impacts of model resolution and coastal topography. Global Biogeochem. Cycles 28, 371–385, doi:10.1002/2013GB004683.

Fine, R.A., et al., 2017. A new look at ocean ventilation time scales and their uncertainties. J. Geophys. Res. Oceans 122, 3771–3798. doi:10.1002/ 2016JC012529.

Giering, S L C., et al., 2017. Particle flux in the oceans: Challenging the steady state assumption. Global Biogeochem. Cycles 31, 159–171. doi:10.1002/2016GB005424.

Gómez-Ocampo, E., et al., 2018. Effects of the 2013-2016 warm anomalies on the California Current phytoplankton. Deep-Sea Res. II 151, 64–76. https://doi.org/10.1016/j.dsr2.2017.01.005.

Grabowski, E., et al., 2019. Coupling carbon and energy fluxes in the North Pacific Subtropical Gyre. Nat. Commun. 10, 1895. https://doi.org/10.1038/s41467-019-09772-z.

Hartman, S.E., et al., 2010. Seasonal and inter-annual biogeochemical variations in the Porcupine Abyssal Plain 2003–2005 associated with winter mixing and surface circulation. Deep-Sea Res. II 57 (15), 1303-1312. https://doi.org/10.1016/j.dsr2.2010.01.007.

Henson, S., Lampitt, R., Johns, D., 2012.Variability in phytoplankton community structure in response to the North Atlantic Oscillation and implications for organic carbon flux. Limnol. Oceanogr. 57(6), 1591–1601. https://doi.org/10.4319/lo.2012.57.6.1591.

Hodur, R.M., et al., 2002. The Coupled Ocean/Atmosphere Mesoscale Prediction System (COAMPS). Oceanog. 15, 88–98. https://doi.org/10.5670/oceanog.2002.39.

Kelly, T.B., et al., 2018. CCE II: Spatial and interannual variability in export efficiency and the biological pump in an eastern boundary current upwelling system with substantial lateral advection. Deep-Sea Res. I 140, 14-25. https://doi.org/10.1016/j.dsr.2018.08.007.

Khatiwala, S., Primeau, F., Holzer, M., 2012. Ventilation of the deep ocean constrained with tracer observations and implications for radiocarbon estimates of ideal mean age. Earth Planet. Sci. Lett. 325–326, 116–125. https://doi.org/10.1016/j.epsl.2012.01.038.

Kishi, M.J., et al., 2007. NEMURO – A lower trophic level model for the North Pacific marine ecosystem. Ecol. Modell. 202, 12–25. doi:10.1016/j.ecolmodel.2006.08.021.

Kuhnz, L.A., et al., submitted, Benthic megafauna assemblage change over three decades in the abyss: Variations from species to functional groups. This volume.

Kwon, E.Y., Primeau, F., Sarmiento, J.L., 2009. The impact of remineralization depth on the air-sea carbon balance. Nat. Geosci. 2(9), 630–635. doi:10.1038/ngeo612.

Lampitt, R.S., et al., 2010. Long-term variability of downward particle flux in the deep northeast Atlantic: Causes and trends. Deep-Sea Res. II 57, 1346-1361. https://doi.org/10.1016/j.dsr2.2010.01.011.

Lombard, F., 2019. Globally Consistent Quantitative Observations of Planktonic Ecosystems. Front. Mar. Sci., https://doi.org/10.3389/fmars.2019.00196.

Lilly, L.E., Ohman, M.D., 2018. CCE IV: El Nino-related zooplankton variability in the southern California Current System. Deep-Sea Res I 140, 36-51. https://doi.org/10.1016/j.dsr.2018.07.015.

Marsay, C.M., et al., 2015. Attenuation of sinking particulate organic carbon flux through the mesopelagic ocean. Proc. Natl. Acad. Sci. USA 112, 1089–1094. https://doi.org/10.1073/pnas.1415311112.

Madin, L.P., 1982. Production, composition and sedimentation of salp fecal pellets in oceanic waters. Mar. Biol. 67, 39–45. https://doi.org/10.1007/BF00397092.

Martin, J.H., Knauer, G.A., Karl, D.M., Broenkow, W.W., 1987. VERTEX: Carbon cycling in the northeast Pacific. Deep-Sea Res A 34(2), 267–285. https://doi.org/10.1016/0198-0149(87)90086-0.

Mayor, D.J., et al., 2014. Microbial gardening in the ocean's twilight zone: detritivorous metazoans benefit from fragmenting, rather than ingesting, sinking detritus: fragmentation of refractory detritus by zooplankton beneath the euphotic zone stimulates the harvestable production of labile and nutritious microbial biomass. Bioessays 36(12), 1132-1137. doi:10.1002/bies.201400100.

McDonnell, A.M.P., Buesseler, K.O., 2010. Variability in the average sinking velocity of marine particles. Limnol. Oceanogr. 55, 2085-2096. doi:10.4319/lo.2010.55.5.2085.

Messié, M., Chavez, F.P., 2017. Nutrient supply, surface currents, and plankton dynamics predict zooplankton hotspots in coastal upwelling systems. Geophys. Res. Lett. 44, 8979-8986. doi:10.1002/2017GL074322.

Monroy, P., Drótos, G., Hernández-García, E., López, C., 2019. Spatial Inhomogeneities in the Sedimentation of Biogenic Particles in Ocean Flows: Analysis in the Benguela Region. J. Geophys. Res. 124(7), 4744-4762. https://doi.org/10.1029/2019JC015016.

Moore, A.M., et al., 2011a. The Regional Ocean Modeling System (ROMS) 4-dimensional variational data assimilation systems. Part I: System overview and formulation. Prog. Oceanogr. 91, 34-49. https://doi.org/10.1016/j.pocean.2011.05.004.

Moore, A.M., et al., 2011b. The Regional Ocean Modeling System (ROMS) 4-dimensional variational data assimilation systems. Part II: Performance and application to the California Current System. Prog. Oceanogr. 91, 50–73. https://doi.org/10.1016/j.pocean.2011.05.003.

Moore, A.M., et. al., 2013. A 4D-Var Analysis System for the California Current: A Prototype for an Operational Regional Ocean Data Assimilation System, in: Data Assimilation for Atmospheric, Oceanic and Hydrological Applications, Vol. II. Springer, Liang Xu and Seon Park (Eds). Chapter 14, pp.345-366.

Pyper, B.J., Peterman, R.M., 1998. Comparison of methods to account for autocorrelation in correlation analyses of fish data. Can. J. Fish. Aquat. Sci. 55, 2127–2140.

Robinson, C., et al., 2010. Mesopelagic zone ecology and biogeochemistry - a synthesis. Deep-Sea Res. II 57(16), 1504-1518. doi:10.1016/j.dsr2.2010.02.018.

Robinson, J., et al., 2017. Far-field connectivity of the UK's four largest marine protected areas: Four of a kind? Earth's Future 5, 475–494. doi:10.1002/2016EF000516.

Ruhl, H.A., et al., 2014. Links between deep-sea megafauna respiration and community dynamics. Ecology 95, 1651-1662. https://doi.org/10.1890/13-0675.1.

Ruhl, H.A, Ellena, J.A., Smith, Jr., K.L., 2008. Connections between climate, food limitation, and carbon cycling in abyssal sediment communities: a long time-series perspective. Proc. of Nat. Acad. Sci USA 105, 17006–17011. https://doi.org/10.1073/pnas.0803898105.

Shanks, A.L., Trent, J.D., 1980. Marine snow: sinking rates and potential role in vertical flux. Deep-Sea Res. A 27(2), 137-143. doi:10.1016/0198-0149(80)90092-8.

Shchepetkin, A.F., McWilliams, J.C., 2004. The regional oceanic modeling system (ROMS): a split explicit, free-surface, topography-following-coordinate oceanic model. Ocean Model. 9, 347–404. https://doi.org/10.1016/j.ocemod.2004.08.002.

Siegel, D.A., et al. 2014. Global assessment of ocean carbon export by combining satellite observations and food-web models. Glob. Biogeochem. Cycles 28, 181–196, doi:10.1002/2013GB004743.

Siegel, D.A., Deuser, W.G., 1997. Trajectories of sinking particles in the Sargasso Sea: modeling of statistical funnels above deep-ocean sediment traps. Deep-Sea Res. I 44, 9–10, 1519-1541. https://doi.org/10.1016/S0967-0637(97)00028-9.

Siegel, D.A., Fields, E., Buesseler, K.O., 2008. A bottom-up view of the biological pump: Modeling source funnels above ocean sediment traps. Deep-Sea Res. I 55, 108–127. https://doi.org/10.1016/j.dsr.2007.10.006.

Smith, K.L., Jr., et al., 2016. Decadal change in sediment community oxygen consumption in the abyssal northeast Pacific. Aquat. Geochem. 22, 401–417. https://doi.org/10.1007/s10498-016-9293-3

Smith, K.L., Jr, et al. 2014. Large salp bloom export from the upper ocean and benthic community response in the abyssal northeast Pacific: Day to week resolution. Limnol. Oceanog. 59: 745–757. https://doi.org/10.4319/lo.2014.59.3.0745.

Smith, K.L., Jr, et al., 2018. Surface ocean to abyssal depth carbon cycling in the NE Pacific; underestimated pulse events during long time-series. Proc. Nat. Acad. Sci. USA. 115 (48), 12235-12240. https://doi.org/10.1073/pnas.1814559115.

Smith, K.L., Jr, et al., 2008. Tracing abyssal food supply back to upper-ocean processes over a 17-year time series in the northeast Pacific. Limnol. Oceanog. 53, 2655–2667. https://doi.org/10.4319/lo.2008.53.6.2655.

Snelgrove, P.V.R., et al., 2018. Global Carbon Cycling on a Heterogeneous Seafloor. Trends Ecol. and Evol. 33, 96-105. https://doi.org/10.1016/j.tree.2017.11.004.

Soltwedel, T., et al., 2016. Natural variability or anthropogenically-induced variation? Insights from 15 years of multidisciplinary observations at the arctic marine LTER site HAUSGARTEN. Ecol. Ind. 65, 89-102. https://doi.org/10.1016/j.ecolind.2015.10.001.

Stemmann, L., Jackson, G.A., Gorsky, G. (2004). A vertical model of particle size distributions and fluxes in the midwater column that includes biological and physical processes—Part II: application to a three year survey in the NW Mediterranean Sea. Deep-Sea Res. I 51(7), 885-908. doi:10.1016/j.dsr.2004.03.002. https://doi.org/10.1016/j.dsr.2004.03.002.

Stukel, M.R. et al. 2017. Mesoscale ocean fronts enhance carbon export due to gravitational sinking and subduction. Proc. Nat. Acad. Sci. USA 114, 1252-1257. https://doi.org/10.1073/pnas.1609435114.

Stukel, M.R., et al. 2019. The Carbon:^{234}Thorium ratios of sinking particles in the California current ecosystem 1: relationships with plankton ecosystem dynamics. Mar. Chem. 212, 1-15. doi: 10.1016/j.marchem.2019.01.003.

Taucher, J., et al., 2014. The viscosity effect on marine particle flux: A climate relevant feedback mechanism. Glob. Biogeochem. Cycles 28, 415–422, doi:10.1002/2013GB004728.

Thomsen, L. et al., 2017 The oceanic biological pump: rapid carbon transfer to depth at continental margins during winter. Scientific Reports 7, 10763. https://doi.org/10.1038/s41598-017-11075-6.

Turner, J.T., 2015. Zooplankton fecal pellets, marine snow, phytodetritus and the ocean’s biological pump. Prog. Oceanog. 130, 205-248. https://doi.org/10.1016/j.pocean.2014.08.005.

Veneziani, M., et al., 2009. A central California coastal ocean modeling study: 1. Forward model and the influence of realistic versus climatological forcing. J. Geophys. Res. 114, C04015. doi:10.1029/2008JC004774.

Villa-Alfageme, M., et al. 2016. Geographical, seasonal and depth variation in sinking particle speeds in the North Atlantic. Geophys. Res. Lett. 43, 8609–8616, doi:10.1002/2016GL069233.

Wei, C.-L., et al. 2012. Standing stocks and body size of deep-sea macrofauna: Predicting the baseline of 2010 Deepwater Horizon oil spill in the northern Gulf of Mexico. Deep-Sea Res. I 69, 82–99. https://doi.org/10.1016/j.dsr.2012.07.008.

Wekerle C, et al. 2018. Properties of Sediment Trap Catchment Areas in Fram Strait: Results From Lagrangian Modeling and Remote Sensing. Front. Mar. Sci. 5, 407. doi:10.3389/fmars.2018.00407.

Wilson, S.E., Ruhl, H.A., Smith, Jr., K.L., 2013. Zooplankton fecal pellet flux in the abyssal northeast Pacific: a 15 year time-series study. Limnol. Oceanog. 58, 881-892. https://doi.org/10.4319/lo.2013.58.3.0881.
Yool, A., Popova, E.E., Anderson, T.R., 2013. MEDUSA-2.0: An intermediate complexity biogeochemical model of the marine carbon cycle for climate change and ocean acidification studies. Geosci. Model Dev. 6, 1767–1811. doi:10.5194/gmd-6-1767-2013.
Yool, A., et al., 2017. Big in the benthos: Future change of seafloor communities in a global-scale, body size-resolved model. Glob. Change Biol. 23, 3554-3566. https://doi.org/10.1111/gcb.13680.
Yoon, W.D., Kim, S.K., Han, K.N., 2001. Morphology and sinking velocities of fecal pellets of copepod, molluscan, euphausiid, and salp taxa in the northeastern tropical Atlantic. Mar. Biol. 139, 923–928. https://doi.org/10.1007/s002270100630.

Table 1. Correlations between sediment trap POC flux, rover chamber estimates of SCOC, and various estimations of EF from source locations resulting from 50, 100 and 1000 m d^{-1}, including 50 and 100 km radius integrations of EF from the source locations, as well as averages using different weighting factors. The p-values have been corrected issues arising serial autocorrelation using the approach of Pyper and Peterman (1998) to adjust the degrees of freedom.

Variables	SCOC	n	effective n	*p*-value	POC flux	n	effec
SCOC	-	-	-	-	0.46	39	16
POC flux	0.46	39	16.6	0.076	-	-	
EF 50 km, 50 m d^{-1}	0.46	49	19.9	0.046	0.39	58	23
EF 100 km, 50 m d^{-1}	0.45	49	20.8	0.044	0.38	58	24
EF 50 km, 100 m d^{-1}	0.62	49	16.5	0.010	0.36	58	19
EF 100 km, 100 m d^{-1}	0.61	49	16.1	0.012	0.40	58	19
EF 50 km, 1000 m d^{-1}	0.48	49	16.2	0.059	0.55	58	19
EF 100 km, 1000 m d^{-1}	0.54	49	15.3	0.040	0.48	58	18
EF 50 km, average of speeds	0.57	49	15.6	0.025	0.48	58	18
EF 100 km, average of speeds	0.57	49	15.8	0.027	0.46	58	18
EF 50 km, weighted for peaks from slow flux	0.51	48	17.1	0.038	0.44	58	20
EF 50 km, weighted for peaks from fast flux	0.51	48	14.2	0.061	0.53	58	17
EF 100 km, weighted for peaks from slow flux	0.50	48	17.7	0.043	0.41	58	21
EF 100 km, weighted for peaks from fast flux	0.55	48	14.2	0.042	0.49	58	17
EF 50 km, highest EF of the three speeds	0.53	49	16.1	0.035	0.48	58	19
EF 100 km, highest EF of the three speeds	0.54	49	16.7	0.032	0.45	58	19

Figure Captions

Fig. 1. Sta. M source locations for particles reaching a trap at 3400 m depth, sinking from 100 m depth at 50 m d^{-1}. The colors indicate months of arrival at trap from January to December, 2013-2017 as indicated in the graphical legend.

Fig. 2. Sta. M source locations for particles reaching a trap at 3400 m depth, sinking from 100 m depth at 100 m d^{-1}. The colors indicate months of arrival at trap from January to December, 2013-2017 as indicated in the graphical legend.

Fig. 3. Sta. M source locations for particles reaching a trap at 3400 m depth, sinking from 100 m depth at 1000 m d^{-1}. Note that the spatial extend is less than in Fig. 1 and 2. The colors indicate months of arrival at trap from January to December, 2013-2017 as indicated in the graphical legend.

Fig. 4. Daily Sta. M time series of SCOC at the seafloor, POC flux at 3400 m depth and EF at 100 m depth at potential origins based on a) 50, b) 100 and c) 1000 m d^{-1} sinking speed. The EF series has been time shifted into the future to its corresponding trap arrive time, which is 66 days for 50 m d^{-1}, 33 days for m d^{-1}, and 3 days for the m d^{-1} speed.

Fig. 5. Monthly Sta. M time series of EF at potential origins at 100 m depth based on a) 50, b)100 and c) 1000 m d^{-1} sinking speeds. Also shown are the POC flux from the 3400 m depth sediment trap and SCOC at the seafloor. The EF series has been time shifted into the future to its corresponding trap arrive time, which is 66 days for 50 m d^{-1}, 33 days for m d^{-1}, and 3 days for the m d^{-1} speed. Panel d) plots the Spearman rank correlation coefficients between EF and POC flux, and EF and SCOC for a 13 month moving window over the time series. Panel e) shows the POC flux record from the sediment trap sampling along with the equal weighting average EF flux from the three sinking speeds with a Martin curve model applied to estimate flux at the trap depth (see section 4.2).

Figure 6. Monthly average values of the source locations for the period 2013-2017 in terms of latitude (a) and longitude (b) for the slow 50 m d^{-1} sinking speed, and for the 100 m d^{-1} speed

(c,d), and 1000 m d^{-1} speed (e,f). Also shown are the monthly average EF flux from 100 m depth for the 100 km radius (e), as well as the monthly average POC flux values from the 3400 m sediment trap system (f) and the monthly averages for SCOC at the seafloor (g). Error bars indicate standard deviation.

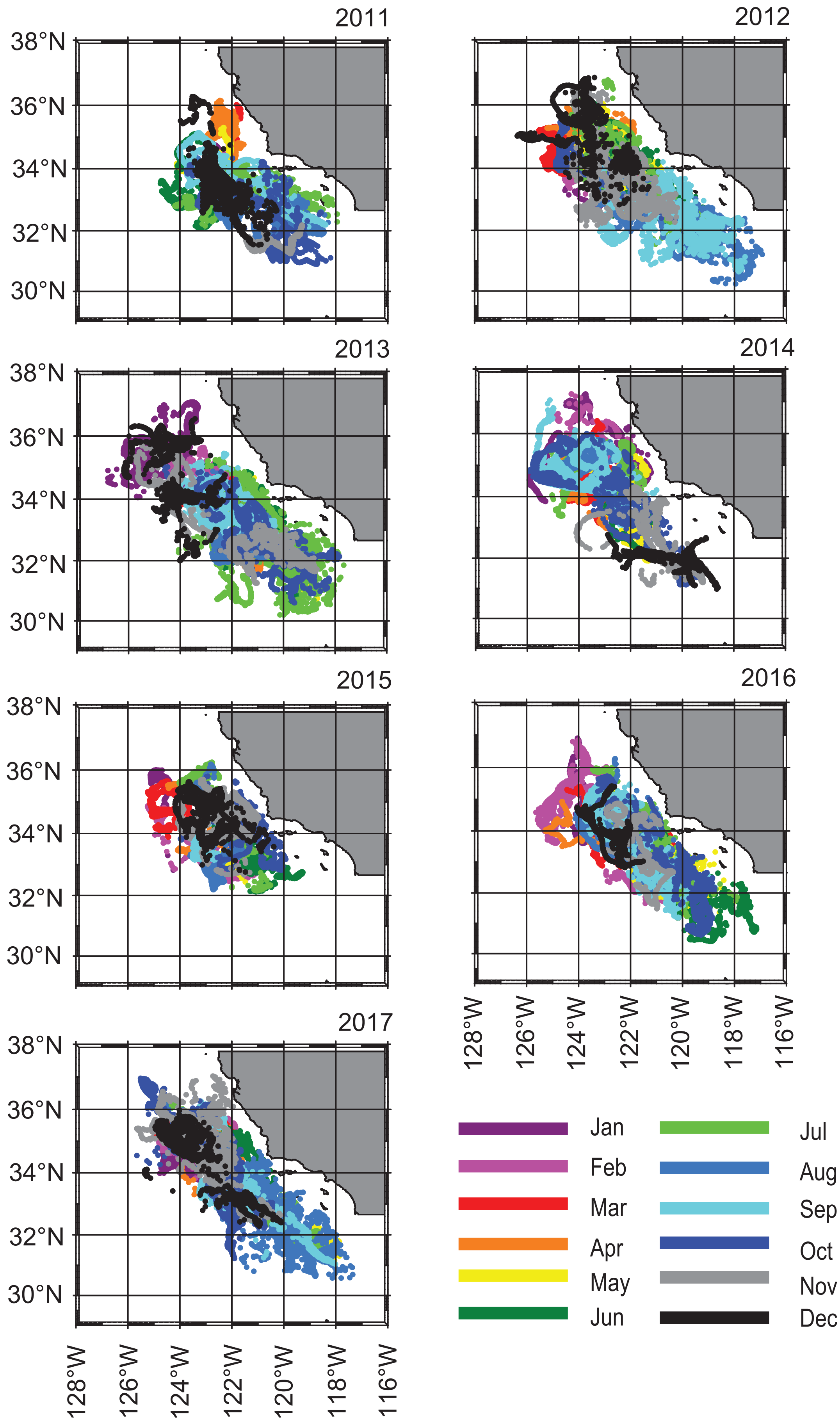
2011
2012
2013
2014
2015
2016
2017
38°N
36°N
34°N
32°N
30°N
128°W
126°W
124°W
122°W
120°W
118°W
116°W
Jan
Feb
Mar
Apr
May
Jun
Jul
Aug
Sep
Oct
Nov
Dec

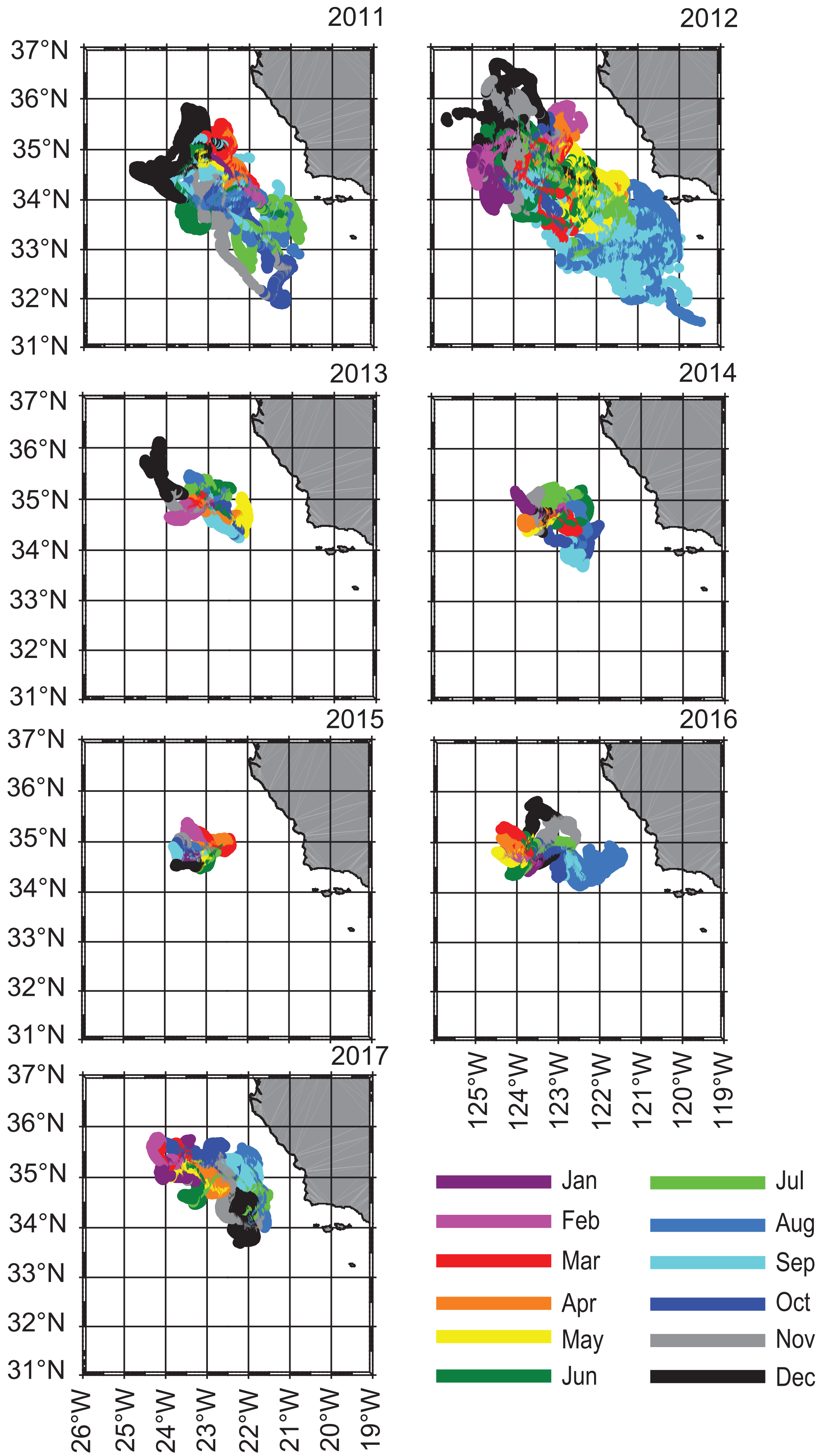
2011
2012
2013
2014
2015
2016
2017
37°N
36°N
35°N
34°N
33°N
32°N
31°N
126°W
125°W
124°W
123°W
122°W
121°W
120°W
119°W
Jan
Feb
Mar
Apr
May
Jun
Jul
Aug
Sep
Oct
Nov
Dec

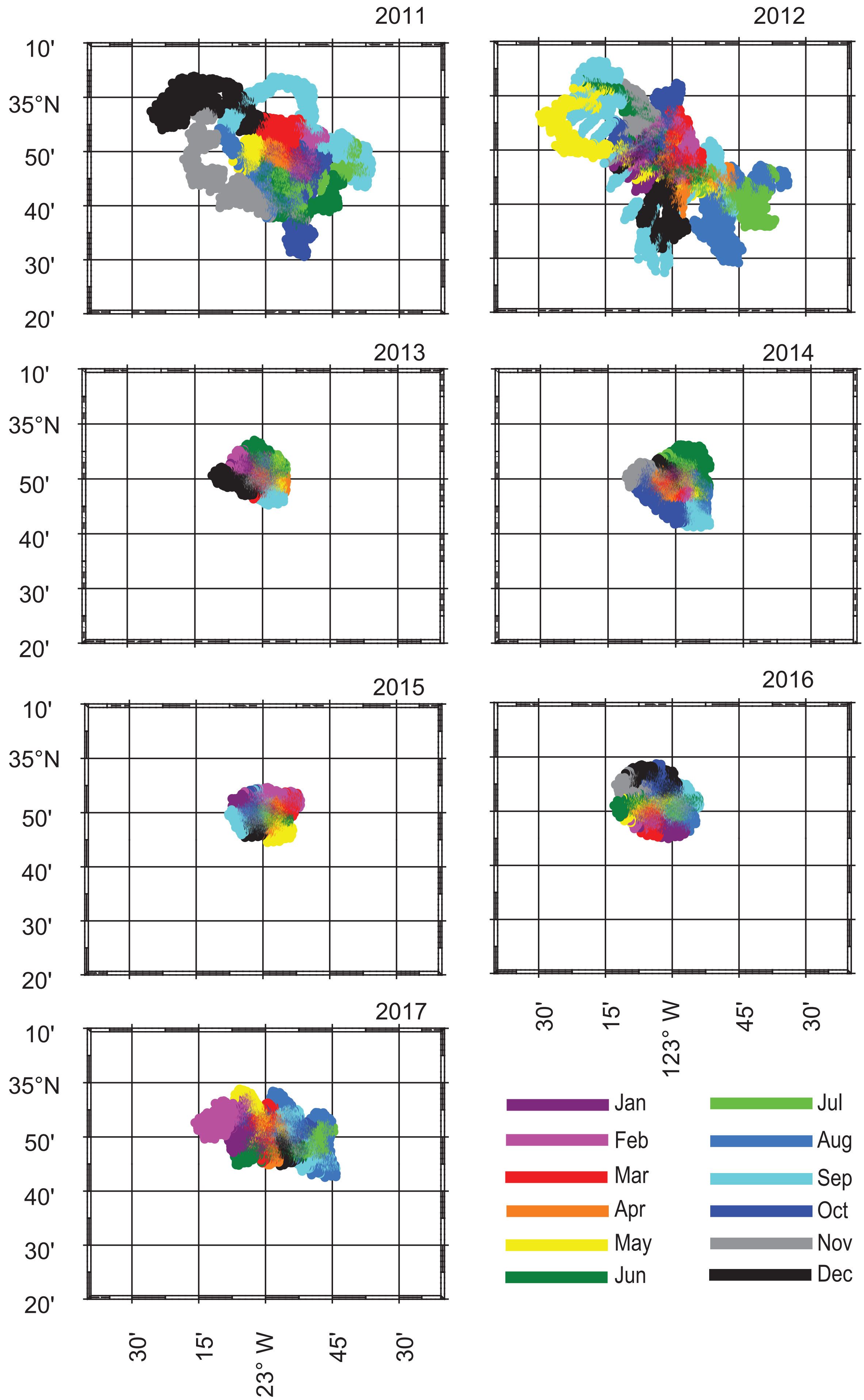
2011
2012
2013
2014
2015
2016
2017
10'
35°N
50'
40'
30'
20'
30'
15'
123° W
45'
30'
Jan
Feb
Mar
Apr
May
Jun
Jul
Aug
Sep
Oct
Nov
Dec

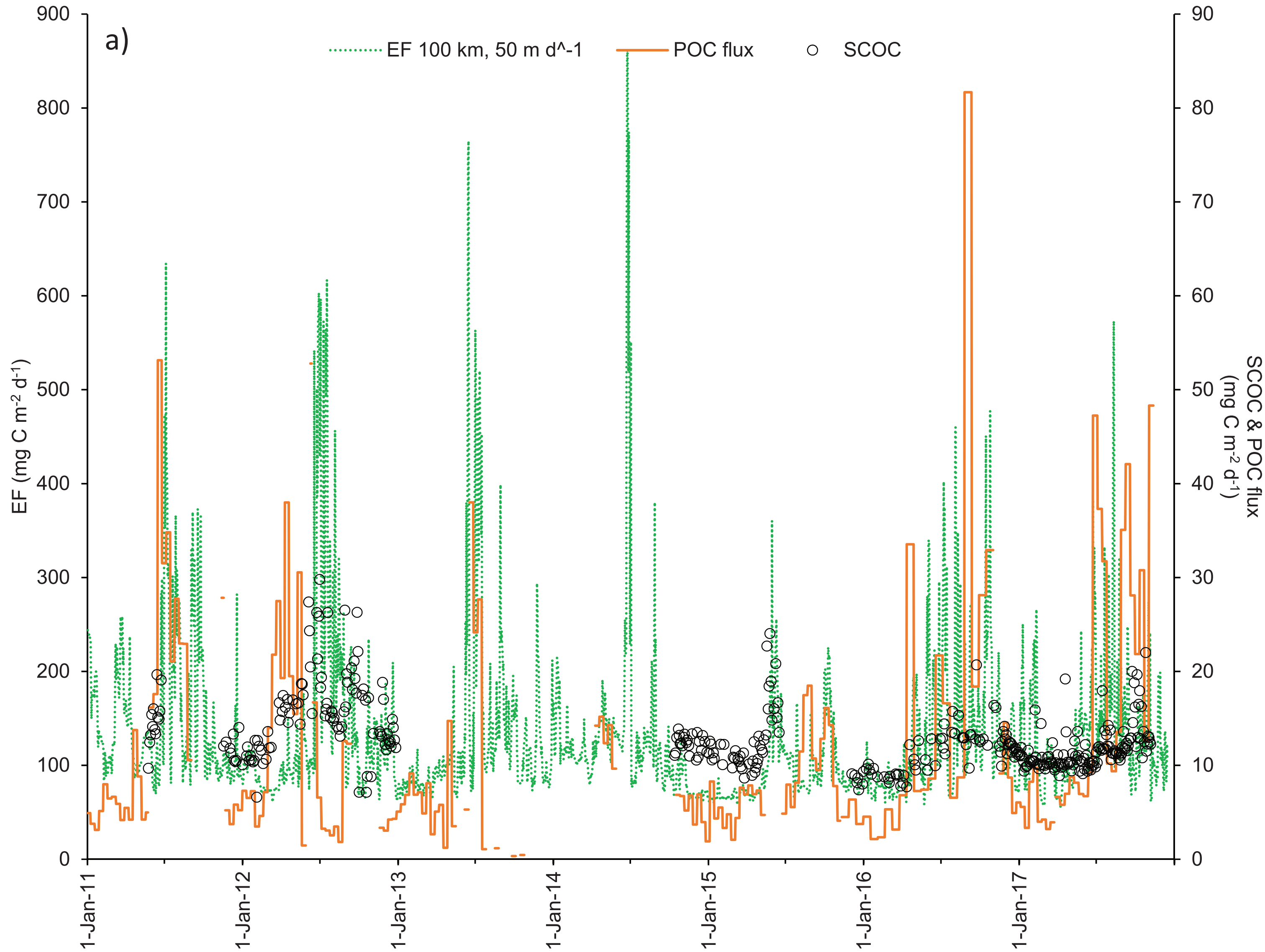
a)
EF 100 km, 50 m d^-1
POC flux
SCOC
EF (mg C m-2 d-1)
SCOC & POC flux (mg C m-2 d-1)
900
800
700
600
500
400
300
200
100
0
90
80
70
60
50
40
30
20
10
0
1-Jan-11
1-Jan-12
1-Jan-13
1-Jan-14
1-Jan-15
1-Jan-16
1-Jan-17

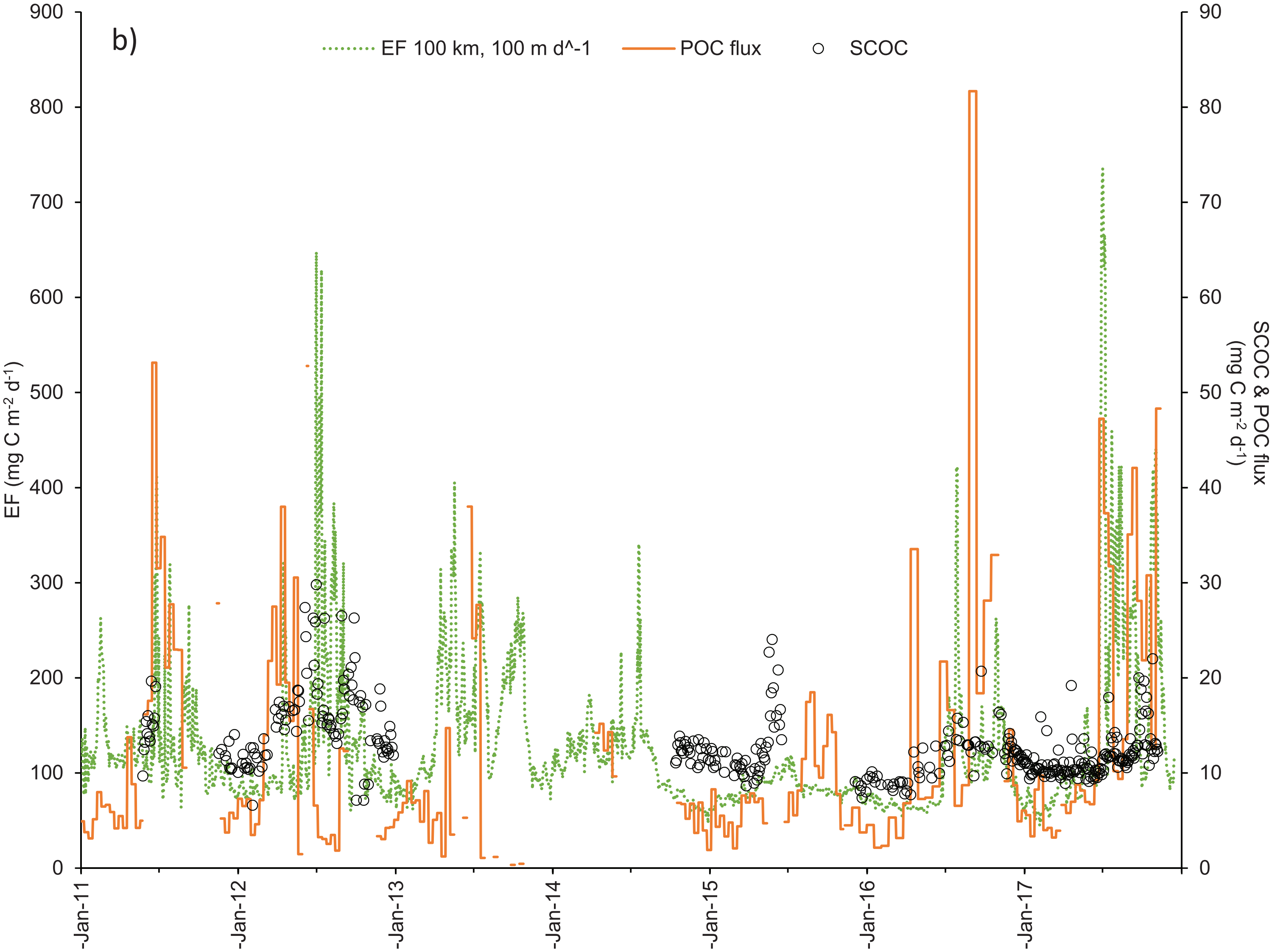

b)
EF 100 km, 100 m d^-1
POC flux
SCOC
EF (mg C m-2 d-1)
SCOC & POC flux (mg C m-2 d-1)
900
800
700
600
500
400
300
200
100
0
90
80
70
60
50
40
30
20
10
0
1-Jan-11
1-Jan-12
1-Jan-13
1-Jan-14
1-Jan-15
1-Jan-16
1-Jan-17

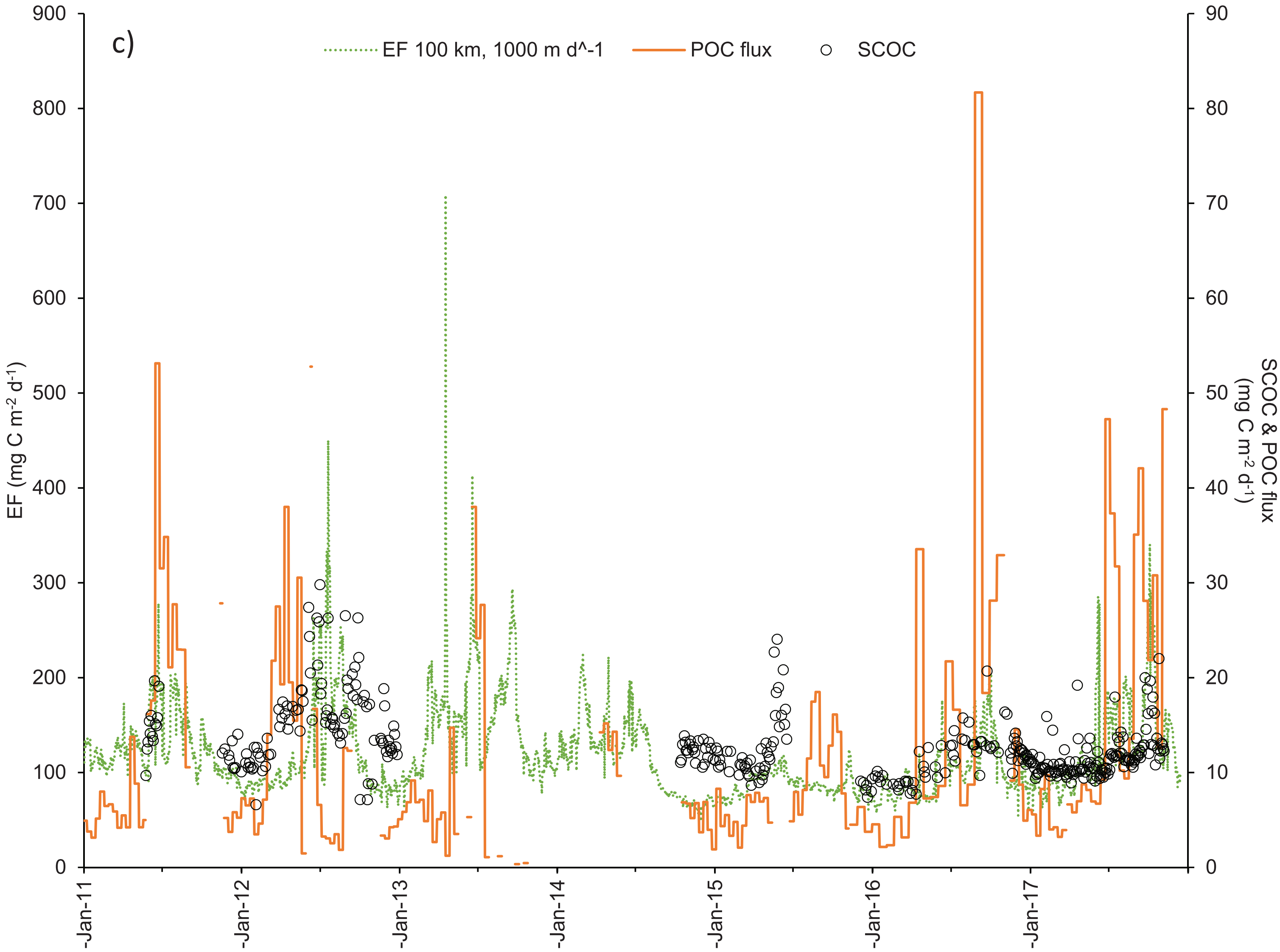

c)
EF 100 km, 1000 m d^-1
POC flux
SCOC
EF (mg C m-2 d-1)
SCOC & POC flux (mg C m-2 d-1)
0
100
200
300
400
500
600
700
800
900
10
20
30
40
50
60
70
80
90
1-Jan-11
1-Jan-12
1-Jan-13
1-Jan-14
1-Jan-15
1-Jan-16
1-Jan-17

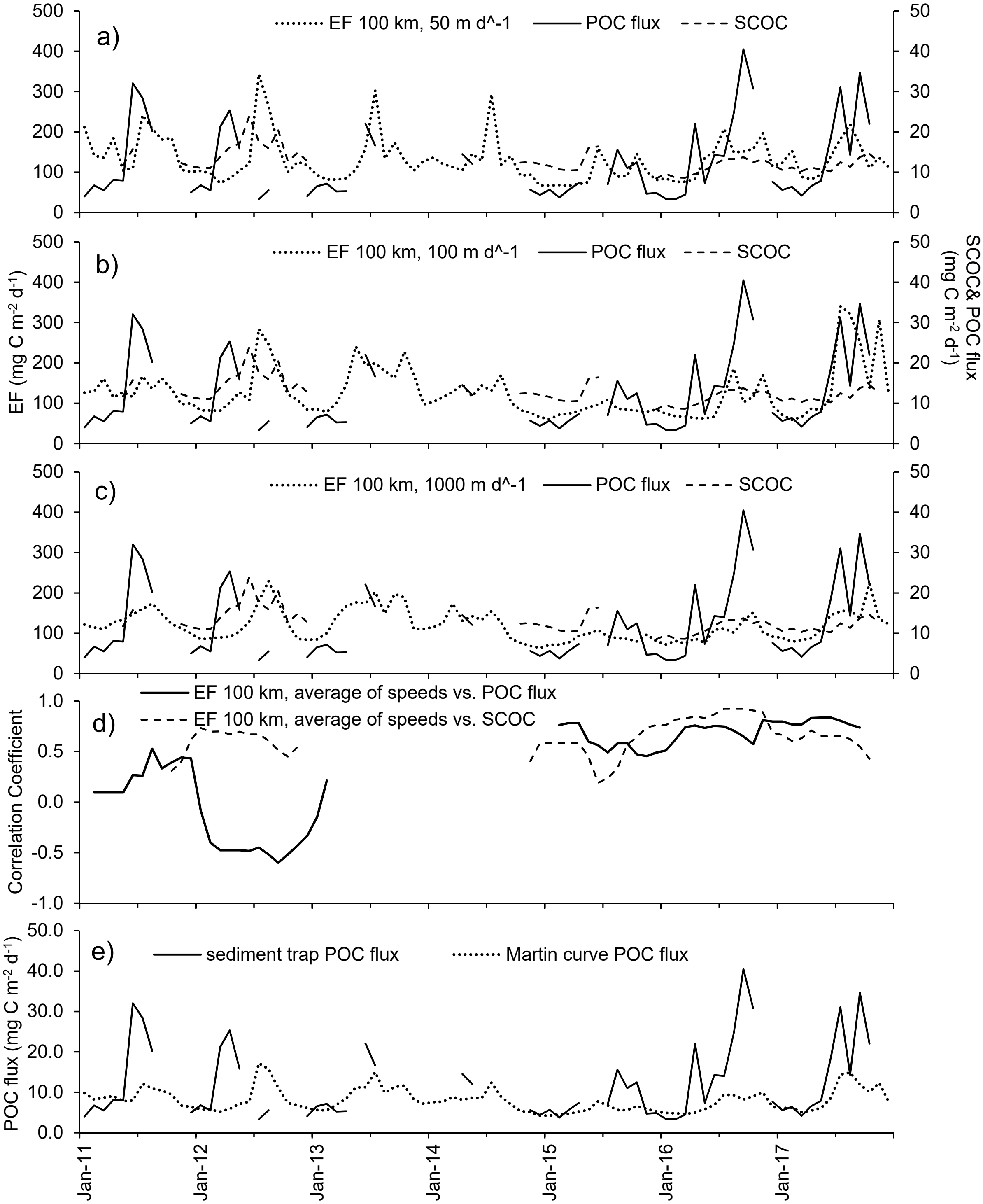
a)
EF 100 km, 50 m d^-1
POC flux
SCOC
b)
EF 100 km, 100 m d^-1
POC flux
SCOC
EF (mg C m-2 d-1)
SCOC& POC flux (mg C m-2 d-1)
c)
EF 100 km, 1000 m d^-1
POC flux
SCOC
d)
EF 100 km, average of speeds vs. POC flux
EF 100 km, average of speeds vs. SCOC
Correlation Coefficient
e)
sediment trap POC flux
Martin curve POC flux
POC flux (mg C m-2 d-1)
Jan-11
Jan-12
Jan-13
Jan-14
Jan-15
Jan-16
Jan-17

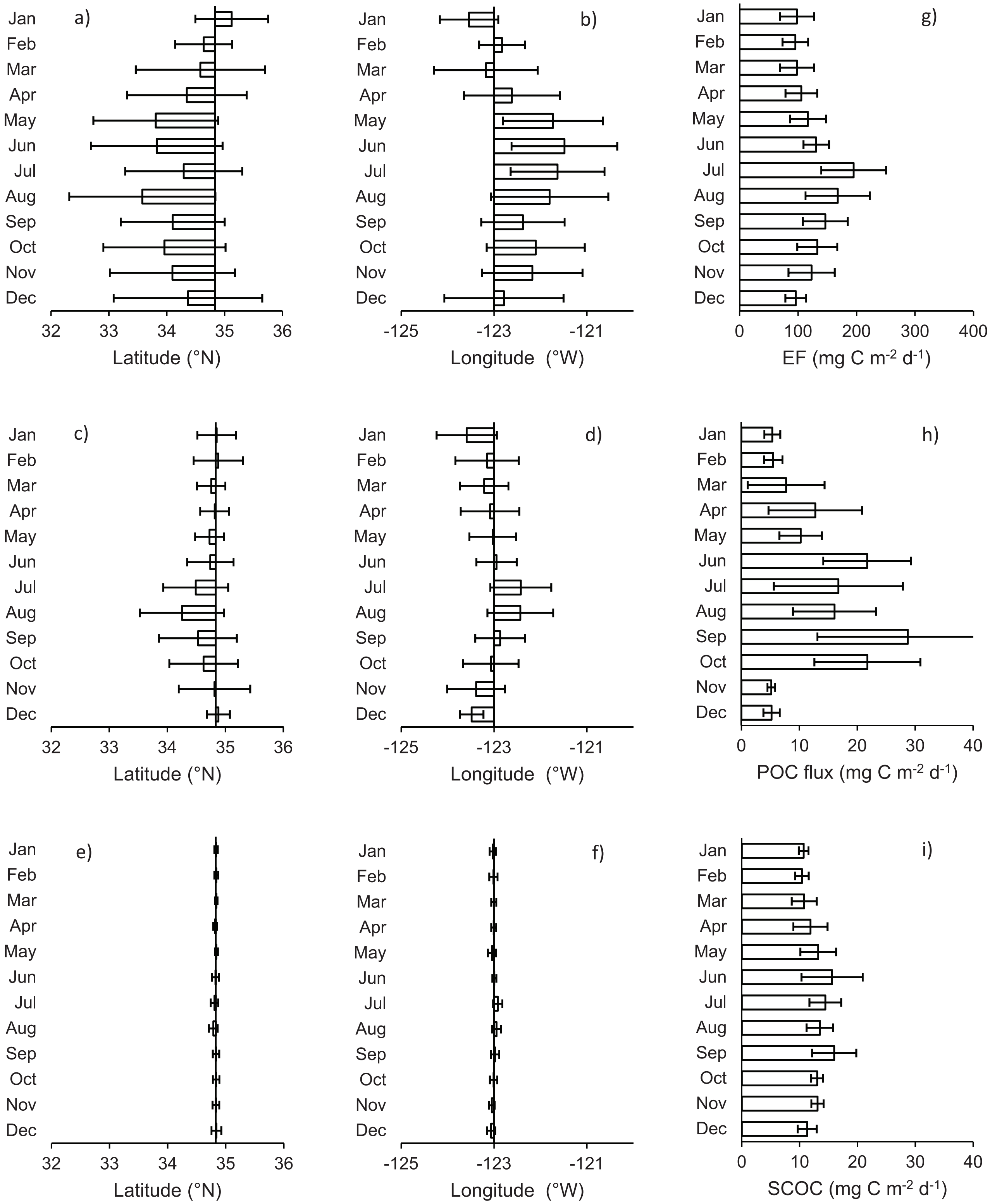
a)
b)
g)
c)
d)
h)
e)
f)
i)
Jan
Feb
Mar
Apr
May
Jun
Jul
Aug
Sep
Oct
Nov
Dec
32 33 34 35 36
Latitude (°N)
-125 -123 -121
Longitude (°W)
0 100 200 300 400
EF (mg C m-2 d-1)
0 10 20 30 40
POC flux (mg C m-2 d-1)
SCOC (mg C m-2 d-1)